Development of a Multi-Energy CT for Small Animals: Characterization of the Quasi-Monochromatic X-Ray Source

Simone Masetti, Michele Fiaschetti, Alessandro Turco, Laura Roma, Pier Luca Rossi, Matteo Mariselli, Nico Lanconelli, and Giuseppe Baldazzi, *Member, IEEE*

Abstract—A new multi-energy CT for small animals is operative (now only in scanning mode) at the Physics Department of the University of Bologna. The system makes use of a set of quasi-monochromatic X-ray beams produced by means of an Highly-Oriented Pyrolytic Graphite Bragg monochromator. This source is able to provide beams with energy tunable in a range from 20 to 70 keV. Here we present a complete characterization of the source. A theoretical model of the source has been analyzed, according to the known Zachariasen's theory for diffracting crystals [1]. The beams have also been characterized in resolution and intensity, over the accessible range, and we present here some measured spectra. The monochromator system demonstrated an energy spread of about 3 keV (Full Width at Half Maximum -FWHM) at a beam energy of 26 keV. At the same energy, the intensity of the output beam is about 6% of the primary beam.

Index Terms—Biomedical X-ray imaging, X-ray, X-ray applications, X-ray imaging, X-ray tomography.

I. INTRODUCTION

X-RAY transmission tomography is very useful for the estimation of attenuation maps in medical imaging. The use of monochromatic radiation has the potential to improve the overall quality of the images, and reduce the dose to patient at the same time. Additional information can be obtained if the data are acquired using more than one energy. In fact, as distinct from conventional radiography, a multi-energy approach can be adopted by using various entrance spectra usually with non-overlapping energies.

It has been demonstrated that monochromatic X-ray beams can be capable of delivering the same image quality at a reduced dose to the patient compared to conventional X-ray tubes [2], [3]. In particular, Boone and Siebert verified this improvement [2] by measuring the image quality with a Figure of Merit defined as a combination of contrast, Signal to Noise Ratio, and dose. In addition, the ability to produce tunable monochromatic

X-rays allows multi-energy analysis. However, it is very challenging to get a monochromatic source with sufficient flux for small animal or human CT [4]–[6]. Our group has gained some experience in the development of quasi-monochromatic X-ray sources with applications in medicine [7]–[9].

The multi-energy approach is an expansion of the method of two-energy radiography. An object is subject to inspection with three (or more) X-ray beams with separated spectral range. By detecting and processing the three (or more) images acquired at the different energies it is possible to estimate some important parameters of the investigated object. For instance, the effective atomic number or the density of the analyzed material can be quantitatively reconstructed. The number of parameters that can be estimated is determined by the number of the energies utilized. A higher number of energies allows to provide more information about the investigated object.

At the Department of Physics of the University of Bologna, we are developing a CT system with a quasi-monochromatic X-ray source for triple-energy small animal studies. Triple-energy projection is an algorithm that combines a set of three quasi-monochromatic images of an object, to obtain a corresponding set of three single-tissue images, which are the density map of three reference materials. The triple-energy technique can be applied to the density-map reconstruction of a contrast medium, as it is able to remove completely the signal of the other tissues (the background noise). In this paper we present a complete characterization of the quasi-monochromatic source based on a Highly-Oriented Pyrolytic Graphite (HOPG) Bragg monochromator.

II. MATERIALS AND METHODS: DESCRIPTION OF THE SYSTEM

Our multi-energy CT system consists of several components: the primary X-ray tube coupled to the Bragg monochromator, the mechanical gantry with rotational and translation axis for providing the CT inspection, and finally the detector for acquiring images at different energies. Fig. 1 shows a picture of the entire system. The system will implement a detector composed of a scintillator coupled to a CCD camera through a 45° mirror. The choice of the scintillator and the camera is still in progress. The multislice detector will cover a Field Of View (FOV) of about 10 cm × 5 cm. The CT inspection will be obtained by a continuous rotation of the gantry (with a rotation of 180 degrees plus the fan beam angle), and after that a discrete translation of the object will be achieved, in order to cover its length. The movement of the gantry (rotation and translation) is

Fig. 1. The multi-energy X-ray system for small animals. The Bragg monochromator is located between the X-ray tube (on the top) and the detector (on the bottom). The gantry with rotational and translation axes is also shown.

Fig. 2. Geometrical characterization of the primary radiation field using a fluorescent screen. The size of the grid is 24 cm × 24 cm.

Fig. 3. The monochromator deployed in our system. The beam from the X-ray tube enters the inner collimator, impinges the HOPG crystal and exits from the outer collimators. Motors for rotating and translating the crystal and for moving the outer collimators are used.

already implemented. Preliminary estimates show that it should be possible to achieve a complete scan of small animals in about 5 minutes.

A. Primary X-Ray Source

The primary X-ray beam is produced by a W-anode tube (RTM 101HS, I.A.E. SpA, Milan, Italy), whose major characteristics are described here. Because of the flux attenuation of the monochromator, we chose a high-performance model: the maximum voltage is 150 kV, and the maximum anodic current is 800 mA. The focal spot size is 0.6 or 0.3 mm, the anodic angular velocities are 3000 rpm or 10000 rpm, and the maximum power dissipated on the anode is 105 kW. The initial high intensity is reduced by Bragg diffraction, and only a fraction of the primary flux (up to 6.5%) is directed to the patient. Given our geometric set-up (source-to-detector distance of about 100 cm, and source-to-object distance of about 90 cm), the resulting unsharpness caused by the focal spot is 0.11 times the focal spot size. Thus, with a focal spot of 600 μm, the unsharpness is limited to less than 70 μm. The primary beam emerging from the tube window is then collimated, in order to reduce the radiation field to the minimum necessary to illuminate the diffraction crystal. Fig. 2 shows an example of the how the radiation field has been geometrically characterized. The position of the inner collimator sets the incidence angle on the crystal, and can be regulated with a micrometric translator.

B. HOPG Bragg Monochromator

The HOPG Bragg monochromator is the heart of the whole system, and is the source for the quasi-monochromatic beam used in multi-energy applications. The performance of such a sour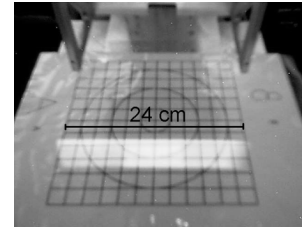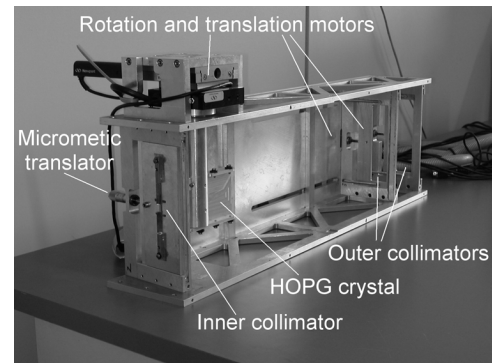ce, in terms of energy-range, energy resolution and photon flux, determines the actual field of application of the multi-energy system. Building on previous experience [8], we have developed an improved version of the monochromator, adding energy selection capability and increasing the intensity of the diffracted beam. The major improvements concern the deployment of an X-ray tube with higher voltage and anodic current, the use of an HOPG crystal with enlarged diffraction surface and the development of a system for automatically controlling the positioning of the crystal and the collimators. Fig. 3 shows a picture of the monochromator used in our system.

The diffraction crystal is an assemblage of three HOPG flat crystals, each one 28 mm × 60 mm × 1 mm, giving a total diffraction surface of 84×60 mm^2. A detailed study based on theoretical models helped us in the system design. A set of spectrometric measurements has subsequently been performed to validate the model prediction and to map the work configurations of the system, where work configuration refers to the ensemble of four parameters related to the position and the rotation of the crystal and to the position of the inner and the outer collimators. This configuration has to be adjusted in order to provide the desired monochromatic beam. We developed an automatic system that calculates the configuration (i.e., the correct value for these four parameters), once the desired energy is fixed. Fig. 4 shows a sketch where the meaning of the two parameters related to the diffracting crystal is illustrated.

The optical scheme adopted allows one to tune the energy of the diffracted beam in a range between 26 keV and 56 keV (first order of diffraction), with fluxes of about 10^7 photons · cm^{-2} · mAs^{-1}. This flux is not constant across the considered energy range, but the variation is limited within one order of magnitude
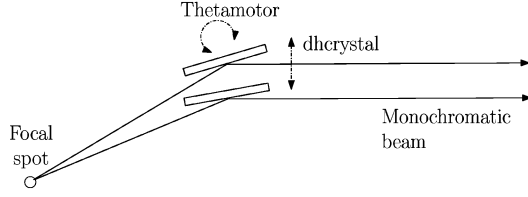
Fig. 4. Sketch showing the path of the beam from the X-ray tube to the exit through the diffracting crystal. The parameters *dhcrystal* and *thetamotor* determine the position and the rotation of the crystal, respectively. They are controlled by the motors shown in Fig. 3.

once the tube voltage is fixed. Higher energies up to 72 keV can be obtained using the second order of diffraction, but the photon flux is reduced by an order of magnitude due to the reduction of the crystal reflectivity. A detailed explanation of the theoretical model used, and of the measurements performed, is presented in the next section.

III. MATERIALS AND METHODS: THE QUASI-MONOCHROMATIC SOURCE

A. Theoretical Model for HOPG

The reference theory for the study of the X-ray reflectivity on mosaic crystals is due to Zachariasen [1]. The model adopted in this work is the *general case of thin mosaic crystal, with primary and secondary extinction*. This model is derived starting from the simpler case of *ideal mosaic crystal*, where the integral reflectivity is expressed as:

$$R_\vartheta = \frac{Q}{2\mu_0} \tag{1}$$

$$Q = r_0^2 \frac{N^2\lambda^3}{\sin 2\vartheta_B} |F|^2 \left(\frac{1+\cos^2 2\vartheta_B}{2}\right) \tag{2}$$

where μ_0 is the linear absorption coefficient of graphite, r_0 is the classical electron radius, λ the incident radiation wave length, F the crystal structure factor, ϑ_B the Bragg angle and N the density of the scattering cells. The reflecting power is defined as the ratio of the diffracted to incident power at the surface of the crystal, and is expressed as:

$$P_{\text{ideal}}(\vartheta) = W(\vartheta_B - \vartheta)\frac{Q}{2\mu_0} \tag{3}$$

where W is an angular distribution function of the glancing angle ϑ. In this work, we adopted for W a Gaussian shape, whose FWHM is the mosaic spread 2α. Fig. 5 shows an example of the reflecting power at a fixed Bragg angle equal to 5 degrees, up to the 3rd order of diffraction. The ideal mosaic model is based upon the hypothesis that the thickness of the crystal is much larger than the mean free path of the incident radiation. This is not our case, because the crystal thickness is 1 mm, while the free path of an X-ray in graphite is about 1 cm at 20 keV. Moreover, the secondary extinction, arising from multiple scattering within the crystal, is small but not negligible. In order to
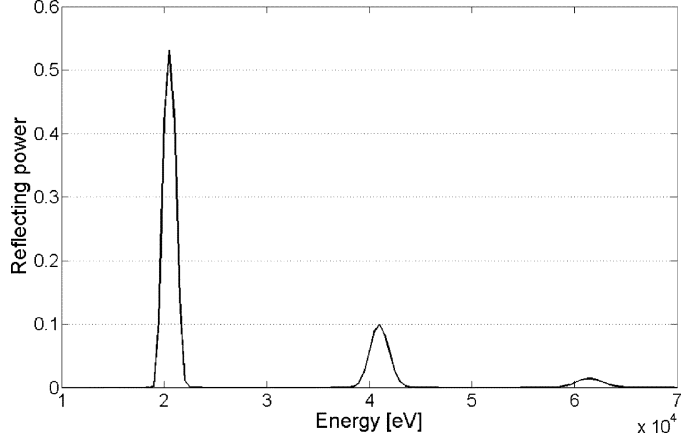

Fig. 5. Reflecting power of HOPG crystal at fixed Bragg angle (5 degrees), up to the 3rd order of diffraction.

take into account the deviation from the ideal case, we use the general expression for reflecting power:

$$P(E,\vartheta)$$
$$= \frac{(WQ+\mu_0) - \sqrt{(WQ+\mu_0)^2 - W^2Q^2}}{WQ}$$
$$\times \left[1 - \frac{U\sin\vartheta\exp(-UT_0)}{(WQ+\mu_0)\sinh(UT_0) + U\sin\vartheta\cosh(UT_0)}\right] \tag{4}$$

where

$$U = \frac{1}{\sin\theta}\sqrt{(WQ+\mu_0)^2 - W^2Q^2}. \tag{5}$$

The first term in formula (4) represents the correction for secondary extinction effects, whereas the second includes the correction for the crystal thickness. The knowledge of the crystal reflecting power $P(E,\vartheta)$ allows one to calculate the spectrum of the diffracted beam, as a function of the incident primary spectrum and of the reflection angle. In fact, if $S_{in}(E,\vartheta)$ is the number of photons having energy between E and $E+dE$, impinging the crystal with an angle ϑ, we can express the number of photons reflected, namely the diffracted beam spectrum $S_{\text{diff}}(E,\vartheta)$, as:

$$S_{\text{diff}}(E,\vartheta) = S_{\text{in}}(E,\vartheta) \cdot P(E,\vartheta). \tag{6}$$

The integral intensity, subsequently, is:

$$I_{\text{diff}}(\vartheta) = \int S_{\text{in}}(E,\vartheta) \cdot P(E,\vartheta)\,dE. \tag{7}$$

It is interesting to define the relative integral intensity $r(\vartheta)$, as the diffracted to incident intensity ratio:

$$r(\vartheta) = \frac{I_{\text{diff}}(\vartheta)}{I_{\text{in}}(\vartheta)} = \frac{\int S_{\text{in}}(E,\vartheta) \cdot P(E,\vartheta)\,dE}{\int S_{\text{in}}(E,\vartheta)\,dE}. \tag{8}$$
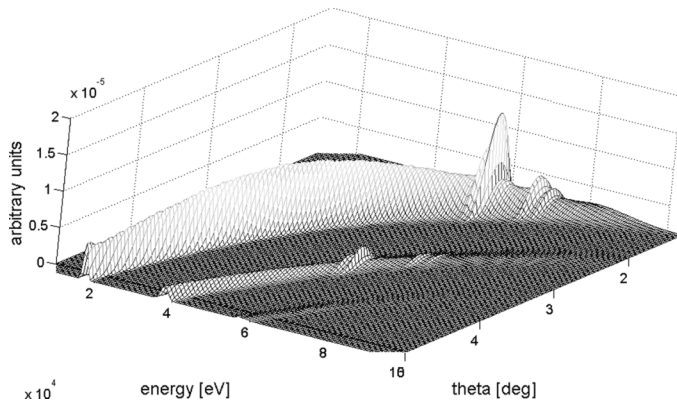
Fig. 6. Model calculation of the HOPG diffracted beam spectrum, for a primary beam at 120 kVp.
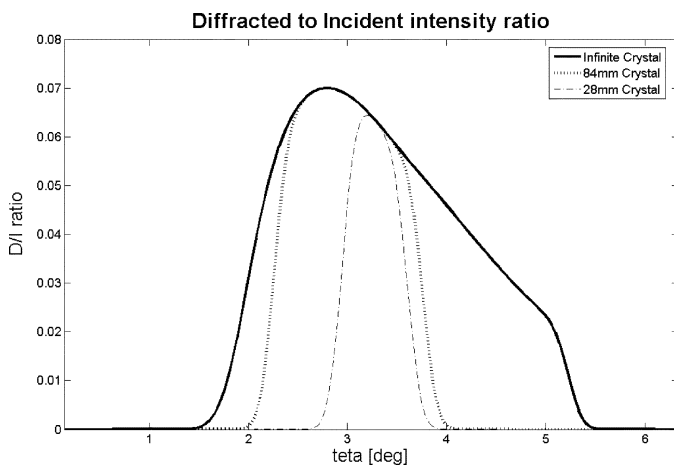

Fig. 7. Examples of diffracted integral intensity ratio, for a crystal angle of 3.3° respect to the optical axis. The minimum and maximum diffraction angles are limited by the crystal length. The current version of the monochromator mounts an 84 mm HOPG crystal.

Formulae (4)–(6)–(7) have been used to calculate the diffracted spectra and intensities. In Fig. 6 we show a diffracted spectrum, as a function of the incident angle and of the diffracted photon energy. An example of relative integral intensities $r(\vartheta)$ is shown in Fig. 7.

B. Experimental Set-Up for Spectrometry of the Beam

The experimental set-up for the spectrometric characterization of the quasi-monochromatic beams is composed of three principal instruments: the X-ray detector XR-100T-CdTe (Amptek, Bedford, MA, USA); the shaping amplifier and power supply PX2T; the multi-channel analyzer MCA8000A.

The XR-100T-CdTe is a high performance X-ray and gamma ray detector, preamplifier, and cooling system based on a $3 \times 3 \times 1$ mm^3 Cadmium Telluride (CdTe) diode detector mounted on a thermoelectric cooler. The internal components are kept at a temperature approximately equal to $-30\,°C$ and can be monitored by a temperature sensitive integrated circuit.

The hermetic package of the detector has a light tight, vacuum tight 100 μm Beryllium window. The PX2T is AC powered and provides all four voltages needed to operate the XR-100T-CdTe
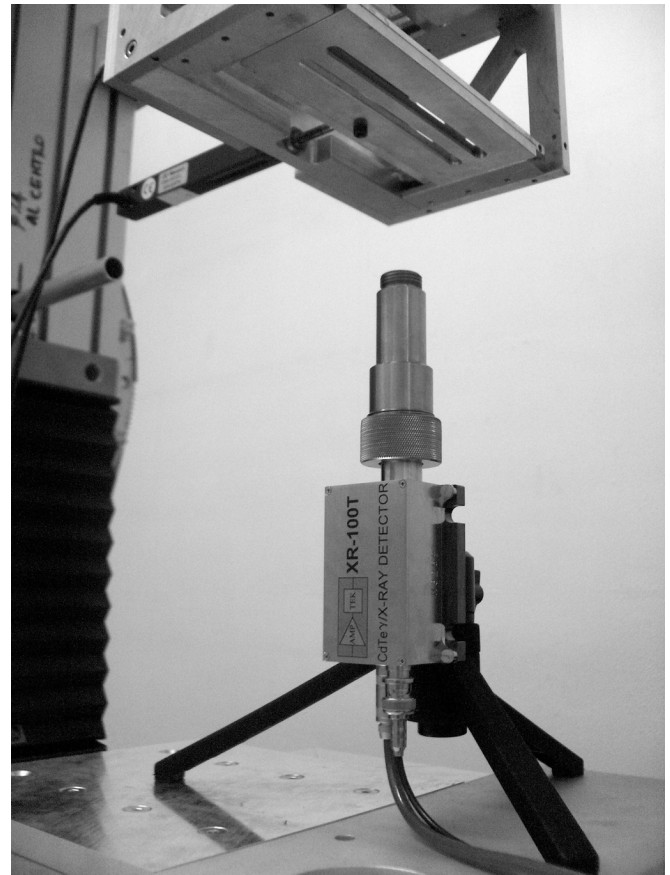

Fig. 8. Spectrometric CdTe detector used for the characterization of the quasi-monochromatic beams.

plus a shaping amplifier. The output from the PX2T can be connected directly to a multi-channel analyzer (MCA). The MCA resolution has been set to 256 channels. The calibration function, which gives the energy corresponding to each channel, has been measured using the characteristic peaks of a radioactive source of ^{241}Am (59.5 keV, 26.3 keV, and 13.95 keV). The Amptek detector has an efficiency greater than 90% for monochromatic energies up to 70 keV (e.g., 99% at 50 keV), and an energy resolution of maximum 1.5 keV (FWHM).

Spectra have been measured in front of the output slit of the monochromator, at a distance of about 80 cm from the focal spot (Fig. 8). Very thin pin-hole tungsten collimators (100 μm and 50 μm) have been used to reduce the flux to the detector.

C. Spectra Analysis and Corrections

The raw spectra obtained from the XR-100T-CdTe have been processed, in order to subtract the background noise. A further correction to take into account the efficiency of CdTe was then performed. Moreover, the effect of the peak distortion typical of the CdTe detectors has been considered [10]. Due to the intrinsic features of the composite semiconductors, this class of X-ray detectors is affected by charge-trapping, and the measured spectra show a distortion called hole-tailing. This effect arises from an incomplete charge collection, due to the trapping of the holes in the crystal defects (trapping sites). The hole-tailing becomes more significant when the energy of the X-rays increases, and

depends on the trapping length of the crystal (mean free path of the charge carriers). In order to correct this effect, the model XR-100T-CdTe is equipped with a Rise Time Pulse Discrimination (RTD) circuit. This circuit analyzes the rising time of the pulse signal, in order to reject events that may be affected by charge trapping. Unfortunately, in our case, because of very high counting rates, the RTD could not be used. Instead, a model based peak reconstruction algorithm has been used to correct the spectra. The algorithm is based upon the Hecht theory [11], and computes the response of the detector to a monochromatic incident beam. The response function is then used to compute the incident spectra from the measured one. We validated the correction algorithm by means of the ^{241}Am source used for the energy calibration.

In addition, the intensity of the beams has been measured using a Barracuda X-Ray Multimeter (RTI electronics, Mölndal, Sweden). We measured the air-kerma of the quasi-monochromatic beams as a function of the peak energy, at fixed distance from the source (80 cm). We computed the ratio of the diffracted beam to the primary beam air-kerma, as compared to the same measurement performed on the W-anode primary beam.

D. *Working Configurations Map of the System*

As previously noted, the beam energy tuning requires a combined motion of translation and rotation of the crystal. Moreover, both the inner and the output collimators must be moved in order to follow the optical axis shift. The complex geometrical relations between the mechanical degrees of freedom of the system have been well investigated, and a dedicated set of measurements have been performed in order to optimize the parameters and maximize the beam quality. As principal outcome, we obtained a map of the optimal configurations. Here, all the mechanical and geometrical parameters are uniquely fixed as a function of a single input: the peak energy at the centre of the beam E_{CF}. These configuration maps have been implemented in software that automatically provides the correct parameters for the selected beam energy E_{CF}, and drives the motors which control all the mechanical elements.

IV. EXPERIMENTAL RESULTS AND DISCUSSION

A. *Characterization of the Beam*

Fig. 9 shows an example of the raw and the corrected spectra, according to the Hecht model, for the 72 keV beam provided by our system. It is worth noting that the offset between the raw and the reconstructed spectrum is due to the incomplete charge collection of the CdTe detector, as previously explained. The corrected spectra obtained have been used to compute the mean energy of the peaks, and the FWHM, as a function of the geometrical parameters of the system. A complete map of working configurations has been designed, in which the value of any degree of freedom (inner collimator, crystal position, rotation angle, output collimators, etc.) is fixed and optimized as a function of the selected mean energy of the beam.

For the first order configurations, the mean energy can be selected with an accuracy of about 0.5 keV in a range from about 26 keV up to 56 keV. This accuracy derives mainly from
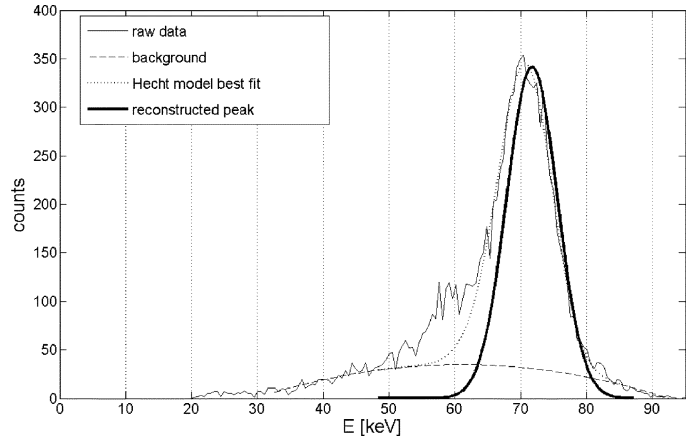

Fig. 9. Hecht model based reconstruction of the 72 keV peak produced by the multi-energy HOPG monochromator (2nd order of diffraction). The first order peak at 36 keV has been suppressed using a Cu filter.
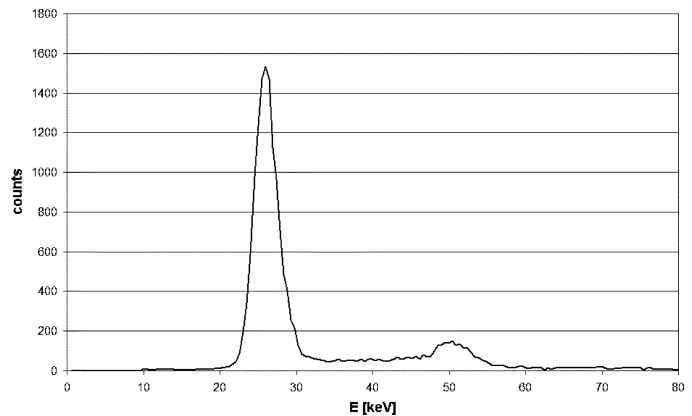

Fig. 10. Acquired spectrum with the first order peak at 26.2 keV (FWHM 2.9 keV) and the second order peak at 52 keV.

the error in the repeatability of the mechanical positioning of the various components of the monochromator. The measured FWHM varies from about 3 keV at the lowest energy to about 7 keV at the highest energy. Fig. 10 shows an example of an acquired spectrum in which we observe the first order peak at 26.2 keV (FWHM 2.9 keV), and the second order peak at 52 keV.

The energy range limits are caused by the mechanical constraints of the system, and can be extended in a future improvement. In particular, the energy range is mainly determined by the maximum translation available for the crystal position (parameter *dhcrystal*), which is 20 mm for our system. Using the second order diffraction harmonics, peaks up to 72 keV have been observed, with FWHM of about 9 keV. In order to have a quasi-monochromatic beam containing only the second order peak, the first order (36 keV) has been suppressed using a filter of 2 mm of Cu. Fig. 11 plots the measured FWHM of the quasi monochromatic beams, for a broad range of energies. We can note that the energy resolution has a nearly linear trend, with respect to the energy of the primary beam.

We also measured the ratio between the air kerma coming from the diffracted beam and the air kerma of the primary beam. The results show a maximum ratio of 6.5% for a peak energy of
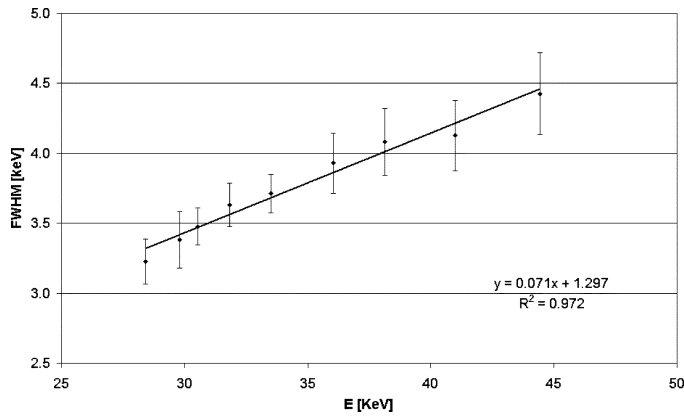
Fig. 11. Characterization of the quasi-monochromatic beams. The plot shows the measured FWHM as a function of the peak energy.
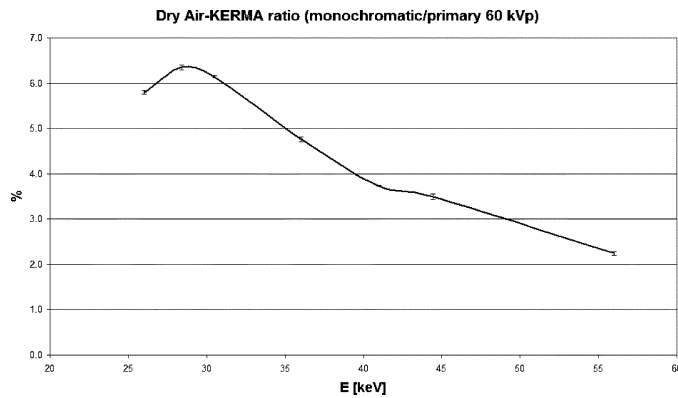

Fig. 12. Diffracted to incident air-kerma ratio of the quasi-monochromatic beams, as a function of the peak energy. The primary W-anode beam was fixed at 60 kVp.
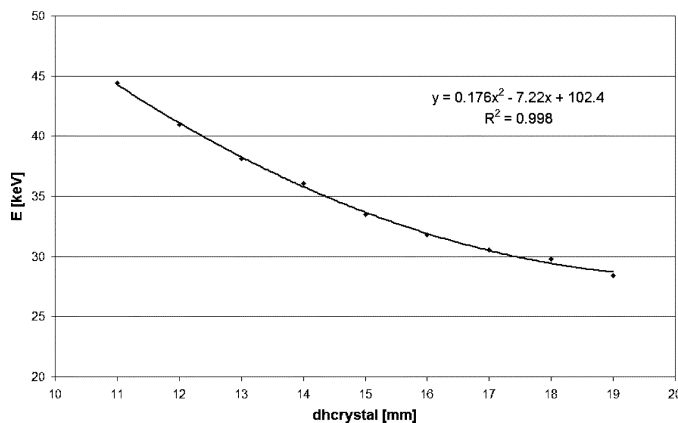

Fig. 13. Example of best-working configuration curve: peak energy at the beam centre E_{CF} as a function of the crystal translation parameter dh_{cryst}. The functional dependence can be inverted to obtain the geometrical parameter as a function of the selected energy.

about 28 keV. Fig. 12 shows this ratio, as a function of the peak energy, for a 60 kVp beam.
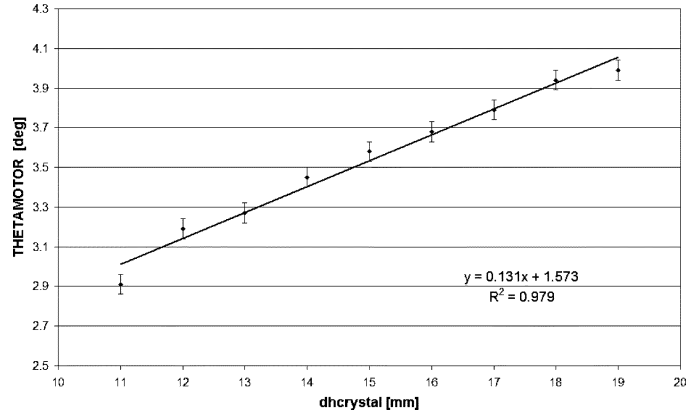

Fig. 14. Example of best-working configuration curve: optimized rotation angle θ_{motor} as a function of the translation parameter of the crystal dh_{cryst}. This relation can be linked to the $E_{CF} -\ dh_{cryst}$ one, to obtain θ_{motor} as a function of E_{CF}.

B. Working Configurations Map of the System

Some examples of best-working configuration curves are illustrated in Figs. 13 and 14. The curve in Fig. 13 represents the peak-energy measured at the centre of the beam E_{CF}, as a function of the crystal shift dh_{cryst}. This relation can be inverted to obtain the value of the crystal translation movement as a function of the selected energy. The curve shown in Fig. 14 is the optimized angular rotation of the crystal ϑ_{motor}, as a function of the crystal shift. The very regular shapes of the calculated relations assure the stability and the repeatability of the system configurations.

V. CONCLUSIONS

We presented a characterization of the quasi monochromatic X-ray source as a part of a CT system for small animals imaging. The monochromator is based on HOPG crystals and supplies beams in the range of energies between 26 keV and 56 keV (first order of diffraction). It presents very good performance, in terms of energy spread (less than 3 keV at 26 keV) and intensity of the beam (up to 6.5% of the primary flux).

In the near future we are going to complete the development of the system, by putting into operation the detector (CCD camera and scintillator). Thus, the multi-energy CT system for small animals will be then fully operational. We will then characterize the detection system with the quasi-monochromatic source, and we'll be able to give an accurate estimate of the scanning time and the dose issues.

REFERENCES

[1] F. Zachariasen, "Theoretical models of diffraction scattering," *Phys. Rep.*, vol. 2, no. 1, pp. 1–75, 1971.

[2] J. M. Boone and J. A. Seibert, "A figure of merit comparison between Bremsstrahlung and monoenergetic X-ray sources for angiography," *J. X-Ray Sci.*, vol. 4, pp. 334–345, 1994.

[3] P. Baldelli, A. Taibi, A. Tuffanelli, M. Gilardoni, and M. Gambaccini, "A prototype of a quasi-monochromatic system for mammography applications," *Phys. Med. Biol.*, vol. 50, pp. 2225–2240, 2005.

[4] A. Rack, S. Zabler, B. R. Muller, H. Riesemeier, G. Weidemann, A. Lange, J. Goebbels, M. Hentschel, and W. Gorner, "High resolution synchrotron-based radiography and tomography using hard X-rays at the BAMline (BESSY II)," *Nucl. Instrum. Meth. A*, vol. 586, pp. 327–518, 2008.

[5] A. Mori, Y. Hayakawa, A. Kidokoro, I. Sato, T. Tanaka, K. Hayakawa, K. Kobayashi, and H. Ohshima, "Measurement of the energy distribution of parametric X-ray radiation from a double-crystal system," *Nucl. Instrum. Meth. B*, vol. 252, pp. 118–123, 2006.

[6] D. J. Crotty, R. L. McKinley, and M. P. Tornai, "Experimental spectral measurements of heavy K-edge filtered beams for x-ray computer mammotomography," *Phys. Med. Biol.*, vol. 52, pp. 603–616, 2007.

[7] C. Avila, J. Lopez, J. C. Sanabria, G. Baldazzi, D. Bollini, M. Gombia, A. E. Cabal, C. Ceballos, A. Diaz Garcia, M. Gambaccini, A. Taibi, A. Sarnelli, A. Tuffanelli, P. Giubellino, A. Marzari-Chiesa, F. Prino, E. Tomassi, P. Grybos, M. Idzik, K. Swientek, P. Wiacek, L. M. Montaño, L. Ramello, and M. Sitta, "Contrast cancellation technique applied to digital X-ray imaging using silicon strip detectors," *Med. Phys.*, vol. 32, no. 12, pp. 3755–3766, 2005.

[8] A. Sarnelli, A. Taibi, A. Tuffanelli, G. Baldazzi, D. Bollini, A. E. Cabal Rodriguez, M. Gombia, F. Prino, L. Ramello, E. Tomassi, and M. Gambaccini, "K-edge digital subtraction imaging based on a dichromatic and compact X-ray source," *Phys. Med. Biol.*, vol. 49, pp. 3291–3305, 2004.

[9] A. Tuffanelli, S. Fabbri, A. Sarnelli, A. Taibi, and M. Gambaccini, "Evaluation of a dichromatic X-ray source for dual-energy imaging in mammography," *Nucl. Instrum. Meth. A*, vol. 489, pp. 509–518, 2002.

[10] S. Miyajima and K. Imagawa, "CdZnTe detector in diagnostic x-ray spectroscopy," *Med. Phys.*, vol. 29, pp. 1421–1429, 2002.

[11] A. Ruzin and Y. Nemirovsky, "Statistical models for charge collection efficiency and variance in semiconductor spectrometers," *J. Appl. Phys.*, vol. 82, no. 6, pp. 2754–2758, 1997.